Validation of full-scale delivered power CFD simulations

Ocean Engineering 238 (2021) 109654

Contents lists available at ScienceDirect

Ocean Engineering

journal homepage: www.elsevier.com/locate/oceaneng

Validation of full-scale delivered power CFD simulations

Michal Orych [a,c,*], Sofia Werner [b], Lars Larsson [a]

[a] Department of Mechanics and Maritime Sciences, Chalmers University of Technology, Gothenburg, Sweden
[b] SSPA AB, Gothenburg, Sweden
[c] FLOWTECH International AB, Gothenburg, Sweden

ARTICLE INFO

Keywords:
Delivered power
Full-scale
Hull roughness
Self-propulsion
Uncertainty
Validation
Verification
CFD

ABSTRACT

Verification and Validation of CFD simulations of delivered power at full-scale are carried out for a single screw cargo vessel. Numerical simulations are performed with a steady-state RANS method coupled with a body force propeller model based on a lifting line theory. There are no significant differences in the uncertainty levels between model and full-scale computations. The finest grid exhibits the numerical uncertainty of 1.40% at full-scale. Computed results are compared with sea trial data for three sister ships. Special attention is paid to the effect of roughness on the hull and propeller. The comparison error for the delivered power is about 1% which is significantly lower than the experimental uncertainty.

1. Introduction

The ship speed-power performance is usually one of the most important factors for a ship operator. At the moment, only model test based predictions are widely accepted for large and expensive projects. In the marine industry computational fluid dynamics, CFD, has been successfully applied to model scale simulations for many years. The availability of validation data, both open and proprietary, makes it relatively easy to develop the best practice and use the method for ship design. It is more difficult to predict the propulsion power at full-scale. In some cases, it is necessary to simulate at the correct Reynolds number due to the flow characteristics, while in other cases the designers wish to achieve better designs without extrapolating from a model scale. Accessible full-scale measurements of good quality are still scarce. Most data comes from sea trials, which are often carried out only at ballast draught, or from monitoring systems on ships in operation. In principle, both can be used for validation purposes. The problems are that the data is most of the time strictly confidential and/or difficult to process due to the uncertainties linked to the measurement accuracy and condition details. In recent years, an increased interest is observed in full-scale simulations. This is due to advancements in numerical methods, more powerful computers as well as trust that the CFD has gained through for example the series of Workshops on CFD in Ship Hydrodynamics initiated in 1980, Hino et al. (2020). However, even as recently as in 2008 (Raven et al., 2008) concluded that a prediction of the full-scale power entirely based on CFD is still not reliable enough when high accuracy is required. The importance of CFD simulations at full-scale was highlighted later in Hochkirch and Mallol (2013) and a practical example illustrated by Kim et al. (2014). In both papers the advantage of full-scale simulations and optimizations of hulls and appendages are shown. Lloyd's Register's full-scale numerical modelling workshop has recently contributed with an open test case for validations. The workshop results were summarized by Ponkratov (2017). Further analysis of the published results, shows that the mean comparison error of the predicted power is 13% for all submitted results and 3 out of 27 participants had errors below 3% for all considered speeds. A thorough study of the numerical accuracy both at model and full-scale can be found in Eça et al. (2010) and Pereira et al. (2017) for a large number of turbulence models without wall functions. However, the papers contain no full-scale validation.

In this work, carefully selected data from an established operator for a large number of sister ships is collected and used for validation. The RANS method, used for simulations, incorporates the wall roughness modelling without the need for wall functions. Therefore, the numerical challenge is greater than the works presented earlier. However, there is also a potential for more accurate predictions. An uncertainty study is presented, which is often lacking in other publications.

The paper first gives a brief introduction to the numerical method used in the code. Thereafter, the case and computational setup are described. The verification, a process which is used to determine numerical errors, is presented. In the validation section only full-scale measurements are used. Model-scale data are not shown for the confidentiality reasons. In connection with the validation, the hull roughness

* Corresponding author at: Department of Mechanics and Maritime Sciences, Chalmers University of Technology, Gothenburg, Sweden.
E-mail address: michal@flowtech.se (M. Orych).

https://doi.org/10.1016/j.oceaneng.2021.109654
Received 3 March 2021; Received in revised form 3 July 2021; Accepted 7 August 2021

Nomenclature

ω	Specific turbulence dissipation
C_F	Frictional resistance coefficient
C_P	Pressure resistance coefficient
C_T	Total resistance coefficient
C_W	Wave resistance coefficient
E	Comparison error
k	Turbulent kinetic energy
K_Q	Torque coefficient
k_S	Equivalent sand grain roughness height
K_T	Thrust coefficient
n	Propeller revolution rate
n_g	Number of grid cells
p	Observed order of accuracy
P_D	Delivered power
U_D	Experimental uncertainty
U_G	Grid uncertainty
U_{SN}	Numerical uncertainty
U_{Val}	Validation uncertainty
w_n	Nominal wake

is discussed and an explanation of the current approach is given. The full-scale delivered power CFD predictions are presented and compared to the collected sea trial measurements. The final section discusses additional errors resulting from the numerical methods, physical modelling and input data.

2. Numerical method

The commercial CFD software SHIPFLOW is used for the simulations. It includes several flow solvers, Broberg et al. (2007). The potential flow solver (XPAN) and the RANS solver (XCHAP) were used in the present study.

XPAN is a non-linear Rankine source panel method, Janson (1997). It uses higher-order panels and singularity distributions. Non-linear boundary conditions are used for the free surface. Dynamic sinkage and trim are computed during the iterative procedure for the non-linear free surface boundary condition. During each iteration, the ship is repositioned and the panellization of the hull and free surface is regenerated.

XCHAP solves the steady, incompressible Reynolds Averaged Navier–Stokes equations using a finite volume method. The explicit algebraic stress turbulence model, EASM, Deng et al. (2005), is used in the present paper. No wall functions are used, and the equations are integrated down to the wall. The equations are discretized using the Roe scheme, Roe (1981), for the convection, while a central scheme is used for the diffusive fluxes. An explicit flux correction is applied to achieve second-order accuracy, Dick and Linden (1992) and Chakravarthy and Osher (1985).

The hull roughness effect is modelled by a modification of the boundary conditions for the specific dissipation of the turbulent kinetic energy, ω and the turbulent kinetic energy, k, Orych et al. (2021). The roughness is quantified using the equivalent sand grain roughness height, k_S .

XCHAP uses structured grids. A single block grid is typically generated for a bare hull case. Multi-block structured or overlapping grids are applied for more complex geometries such as hulls with appendages, and local grid refinements. The solver is flexible in terms of H/C/O grid topologies, and it can handle grid point and line singularities at the boundary surfaces, as well as folded and periodic grids.

To simulate the effect of the propeller, body forces are introduced. When the flow passes through the propeller swept volume, its linear and angular momentum increase as if it had passed a propeller with an infinite number of blades. The forces vary in space, but are independent of time, and generate a propeller induced steady flow. The body forces are computed with a built-in lifting line propeller analysis program, Zhang (1990). Additionally, a friction resistance component is accounted for that contributes to the propeller torque. This simple modelling is also used to take into account the blade roughness.

The computation of the body forces is embedded in an iterative procedure, where first the current approximation of the velocity field is extracted at a representative propeller plane. The effective wake is thereafter obtained by subtracting the induced propeller wake. This is the function of the propeller code and is computed by the circulation from the previous iteration in the lifting line method. The new circulation and forces are computed in the effective wake. Thereafter the forces are distributed over the volume cells in the cylindrical grid. The body forces are added to the right-hand side of the flow equations. This will give a new velocity field after solving the equations. The body forces are updated in every iteration. At convergence, the total wake computed by the RANS solver and the lifting line method should match in the selected propeller plane.

To simulate self-propulsion, the program automatically adjusts the propeller rotational speed to achieve a balance between resistance and thrust. For the model scale simulations, an allowance force can be given or computed according to the 1978 ITTC Performance Prediction Method, ITTC (2017a).

The momentum and continuity equations are solved in a coupled manner, while the turbulent quantities are solved separately. A Krylov type solver from the PETSc software suite, PETSc (2020a), is used to solve the linear equations. The selected GMRES, PETSc (2020b), with the block Jacobi preconditioner, PETSc (2020c), is in this case very efficient, both in terms of convergence speed and stability.

3. Case description

The test case for this validation was carefully selected to get a high-quality reference. It is a conventional single screw cargo vessel with Lpp about 180 m, beam 30 m and block coefficient of 0.78. However, most of the data is confidential. Therefore, not all details can be included in the paper. A full set of towing tank and sea trial measurements is available. The model tests are performed for both resistance and self-propulsion with a hull length of 7 m.

A large number of these ships were built, and the measurements for the validation come from 12 sister ships. This substantially increases the reliability of the full-scale data. The collected measurements were obtained during the sea trials upon delivery from the yard. They are post-processed according to the ITTC procedure for sea trials analysis, ITTC (2017a). Environmental effects such as wind, waves and currents are eliminated for a fair comparison with the numerical predictions, performed with a steady-state code. The design draught and the 12.5 knots speed corresponding to Reynolds number of approximately 8.5×10^6 and 9.6×10^8 in model and full scale respectively are used in the verification computations. For the validation, additional speeds are added, 13.5 and 14.5 knots.

4. Computational setup

The computational setup follows the current best practice for SHIPFLOW. Two different methods are used to obtain the solution. The nonlinear potential flow method, XPAN module, is used to compute the wave pattern, dynamic sinkage and trim. The wave resistance is evaluated using a wave-cut integration method.

The viscous pressure resistance and friction are computed using the RANS method XCHAP. For this computation, an H-O structured background grid describing the hull is complemented with overlapping

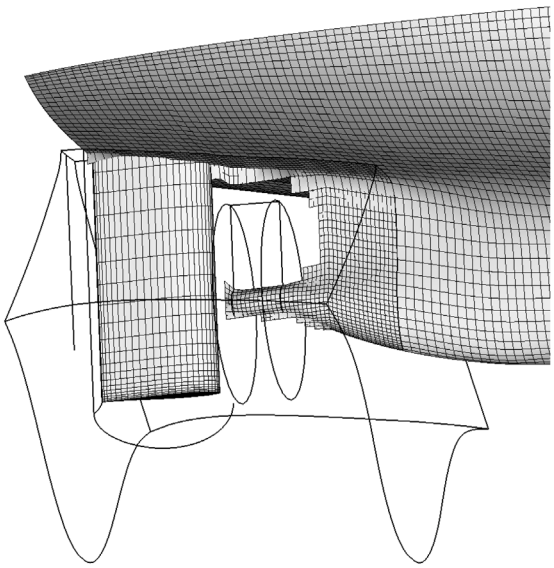

Fig. 1. Overlapping grid assembly. Surface mesh for hull, local refinement and rudder are visualized. Grid block outlines are visible for rudder, local refinement and propeller components.

component grids. The domain extends 0.8 Lpp in front of and behind the hull and the outer radius of the semi-cylindrical domain is 3.0 Lpp. Behind the submerged part of the transom a separate grid block is used. An additional cylindrical domain represents the propeller. The separate rudder grid is of O-O type. Both the propeller and the rudder are encapsulated within a local refinement that is based on the background grid, where each cell is split to generate eight new cells. Bilge keel geometry is not included in the simulations. An example grid assembly is shown in Fig. 1. It should be noted that in the RANS simulations the free surface effects are not taken into account and a double-model approach with a slip boundary condition at the water plane is used. Simulations performed using a viscous free-surface flow variant of the code confirm a limited interaction between the wave pattern and the viscous flow. Therefore, the double-model approximation can be applied in this case. However, the dynamic sinkage and trim computed by the potential flow method is taken into account. A detailed description of the applied boundary conditions is given in Broberg et al. (2007).

The simulations are performed with the fluid properties corresponding to the towing tank test conditions at model scale, and 15 °C seawater at full scale. In both model and full scale, the hull is considered hydraulically smooth in the grid dependency study. The hull roughness modelling at full scale is used in the final validation only.

5. Verification

Verification is carried out to investigate the numerical accuracy. It covers towed and self-propelled cases at a model and full scale. Although, the main focus of the paper is the full-scale, the verification at both scales is presented since there is much more experience from model scale simulations in the ship hydrodynamics community. Therefore, one can easily judge the quality of the presented results. The second reason is that the code behaviour at full scale can be compared to the model scale for reference.

Due to the hybrid RANS and potential flow approach the verification process is divided into numerical uncertainty estimations for the RANS solver and the potential flow solver separately. In all RANS computations, the potential flow meshing is unchanged. A separate test, described in the discussion section, is done to estimate the potential flow mesh sensitivity. This approach is adopted since there might be a reason to question mesh refinement studies for free surface potential flow solvers. The problem is that refining the free surface spatial discretization in a potential flow panel method will lead to the point where breaking waves start appearing. This means that a new physical phenomenon appears in the solution, which cannot be resolved with the potential flow method and causes the solver to fail.

Table 1
Cell sizes in selected regions for the optimized cell distribution, non-dimensionalized with Lpp.

Grid	Length-wise		Girth-wise	y^+
	forebody	aftbody	midship	midship
1	0.58×10^{-3}	0.41×10^{-3}	1.50×10^{-3}	0.495
6	1.38×10^{-3}	0.97×10^{-3}	3.57×10^{-3}	1.177

For the RANS grid dependency study, the calculations are performed in several steps to find the most suitable grid distribution and also to investigate the effect of overlapping grids on the results. Before generating the set of geometrically similar grids the sensitivity of the solution to a varying number of cells in the girth-wise, normal and length-wise directions in several regions along the hull is studied. In this way, a more balanced distribution of cells is found, that provides a good description of the flow without the need to overspend the computational resources. Thereafter, two sets of systematically varied grids are studied for initial and optimized cell distributions. It is found that the results converge with an increasing number of cells to similar values for both sets of grids. However, the optimized one shows monotonic convergence for a lower total amount of cells.

The grid refinement ratio is $\sqrt[4]{2}$ in each direction and the total number of cells range from 2.03×10^6 to 25.54×10^6, and from 3.77×10^6 to 44.14×10^6 at model and full scale respectively. The cell sizes in selected regions for the optimized cell distribution for the finest (#1) and coarsest (#6) grids are given in Table 1. The length and girth-wise sizes are non-dimensionalized by Lpp. It should be noted that the aftbody cell size in the length-wise direction is given in a region where the overlapping grid refinement is used. The number of cells in the normal direction for the full-scale simulations is about 65% larger compared to the model scale, to compensate for the clustering of cells close to the hull, due to the stretching necessary to keep y^+ according to the requirements of the turbulence model.

The simulations are executed for a bare hull grid first, then the rudder and refinement grids are added in subsequent steps. In all cases a similar level of uncertainties is observed, leading to the conclusion that the overlapping grid algorithm has a very limited impact on the overall result quality. One very important observation, that confirms earlier experience, Korkmaz (2015), is that for self-propulsion computations the refinement in the volume surrounding the propeller is necessary to avoid a scatter, visible as an oscillatory grid convergence. If the embedding grid is not fine enough, especially in the axial direction, the insufficiently accurate interpolation of the forces introduced by the propeller leads to increased uncertainty of the propulsive factors.

The least square root, LSR, method is used to determine the numerical uncertainty and the order of accuracy, Eça and Hoekstra (2014). A software tool prepared by MARIN, MARIN (2018), is used to process the results.

5.1. Model scale

The model scale towed condition results are given in Table 2. The total resistance coefficient, as well as frictional and viscous pressure components and nominal wake fraction, are presented. C_F increases, while C_P decreases with grid size, which seems to be a feature of the solver. All variables converge well with limited scatter. In the case of C_F and C_T the observed order of accuracy, p, is above the limit suggested by Eça; hence it is set to 2.0. See, Eça and Hoekstra (2014). The grid uncertainty, U_G, is expressed as a percentage of the solution from the finest grid, S_1.

Table 2
Resistance component coefficients and nominal wake of towed hull, model scale.

Grid	$C_F \times 10^{-3}$	$C_P \times 10^{-3}$	$C_T \times 10^{-3}$	w_n
1	3.043	0.470	3.631	0.2135
2	3.034	0.477	3.628	0.2136
3	3.024	0.480	3.621	0.2145
4	3.002	0.494	3.613	0.2153
5	2.968	0.506	3.592	0.2165
6	2.910	0.522	3.549	0.2175
p	2.0	1.2	2.0	1.5
$U_G\%S_1$	3.1	7.0	1.7	0.9

Table 3
Uncertainty and deviations of total resistance coefficient, model scale.

Grid	$n_g \times 10^6$	$C_T \times 10^{-3}$	$U_G\%S_i$	$\lvert C_{Ti} - C_{T0}\rvert \%C_{T0}$
0	∞	3.652	–	–
1	8.99	3.631	1.7	0.6
2	5.42	3.628	2.1	0.7
3	3.27	3.621	3.0	0.9
4	1.97	3.613	4.3	1.1
5	1.19	3.592	5.8	1.6
6	0.73	3.549	8.2	2.8

Table 4
Resistance component coefficients of self-propelled hull, model scale.

Grid	$C_F \times 10^{-3}$	$C_P \times 10^{-3}$	$C_T \times 10^{-3}$
1	3.150	0.794	4.061
2	3.142	0.800	4.059
3	3.136	0.812	4.065
4	3.124	0.819	4.060
5	3.109	0.851	4.077
6	3.093	0.868	4.077
p	1.4	1.7	1.1
$U_G\%S_1$	1.1	3.6	1.3

Table 3 contains C_T results obtained for all grid sizes, n_g, as well as the value extrapolated to an infinite number of cells. Since it is often not practical to use the finest grid that was included in the verification study, the uncertainties for coarser grids are also very important, here expressed as a percentage of the solution for each grid, S_i. The last column can be of particular interest to the designers. It shows a difference between C_{T0}, the value extrapolated to zero step size, and each grid result, C_{Ti}, in percent of C_{T0}. The total resistance average comparison error, $|E|$%D, is about 1% for all three speeds that are considered.

The propeller action in the self-propulsion case seems to stabilize the flow and the resistance components show lower uncertainty, Table 4. For a better perception of the data, the results are also plotted in Fig. 2. The horizontal axis represents the relative step size between the grids. The resistance coefficients indicate monotonous grid convergence with small uncertainties and limited scatter.

Also, the propulsive factors behave well, and the delivered power converges at a nearly theoretical rate for this method and with small scatter, Table 5.

The deviation from the value extrapolated to the infinitesimally fine grid is 0.15% for the finest grid and the maximum is 0.67% for the second coarsest one, Table 6. The last column shows a difference between the extrapolated value of P_{D0} and each grid result, P_{Di}, in percent of P_{D0}. The same values of $U_G\%S_i$ for all grids are the result of the used verification method and its specific evaluation process. For a detailed description the reader is referred to Eça and Hoekstra (2014).

5.2. Full scale

The resistance components and nominal wake for the "towed" full-scale case are given in Table 7 only for reference, as these quantities are in practice not measured. The uncertainties are at a similar level to those observed at model scale.

Table 5
Propulsive factors, model scale.

Grid	K_T	$K_Q \times 10^{-1}$	n [rps]	P_D [W]
1	0.13885	0.1957	6.576	35.03
2	0.13886	0.1957	6.573	34.99
3	0.13888	0.1958	6.580	35.11
4	0.13930	0.1963	6.564	34.94
5	0.13991	0.1970	6.573	35.21
6	0.14041	0.1975	6.561	35.12
p	2.0	2.0	2.0	1.8
$U_G\%S_1$	1.0	0.8	0.6	2.3

Table 6
Uncertainty and deviations of delivered power, model scale.

Grid	$n_g \times 10^6$	P_D [W]	$U_G\%S_i$	$\lvert P_{Di} - P_{D0}\rvert \%P_{D0}$
0	∞	34.98	–	–
1	25.54	35.03	2.3	0.15
2	15.27	34.99	2.3	0.04
3	9.17	35.11	2.3	0.38
4	5.54	34.94	2.3	0.10
5	3.32	35.21	2.3	0.67
6	2.03	35.12	2.3	0.41

Table 7
Resistance component coefficients and nominal wake of towed hull, full scale.

Grid	$C_F \times 10^{-3}$	$C_P \times 10^{-3}$	$C_T \times 10^{-3}$	w_n
1	1.616	0.257	1.991	0.1270
2	1.612	0.265	1.993	0.1276
3	1.609	0.270	1.996	0.1286
4	1.600	0.289	2.006	0.1304
5	1.593	0.311	2.021	0.1324
6	1.582	0.340	2.039	0.1342
p	1.6	2.0	2.0	1.3
$U_G\%S_1$	0.9	8.7	1.9	3.8

Table 8
Resistance component coefficients of self-propelled hull, full scale.

Grid	$C_F \times 10^{-3}$	$C_P \times 10^{-3}$	$C_T \times 10^{-3}$
1	1.655	0.532	2.304
2	1.650	0.538	2.305
3	1.647	0.549	2.312
4	1.638	0.566	2.321
5	1.629	0.592	2.337
6	1.617	0.619	2.353
p	1.5	1.9	2.0
$U_G\%S_1$	1.1	5.5	1.6

In Table 8 the results from the grid dependence study for resistance components of a self-propelled case are shown. The results are also plotted in Fig. 3. It can be noticed that the scatter at full-scale is not larger than in the model-scale.

Small uncertainties can also be observed for all propulsive factors, see Table 9. Values well below 1% are seen for K_T, K_Q and n.

For the finest grid the delivered power grid uncertainty, $U_G\%S_1$ is 1.4% and the deviation from the extrapolated value, $|P_{D1} - P_{D0}|\%P_{D0}$, is 0.49%, see Table 10.

The results for K_T, K_Q and n are plotted for all grids as a function of the relative grid size in Fig. 4, and P_D in Fig. 5.

All the above verification results are given for a smooth hull. Further calculations with roughness show that the applied modelling does not seem to increase the scatter in the solutions and the uncertainties are very similar, therefore only one set of data is presented.

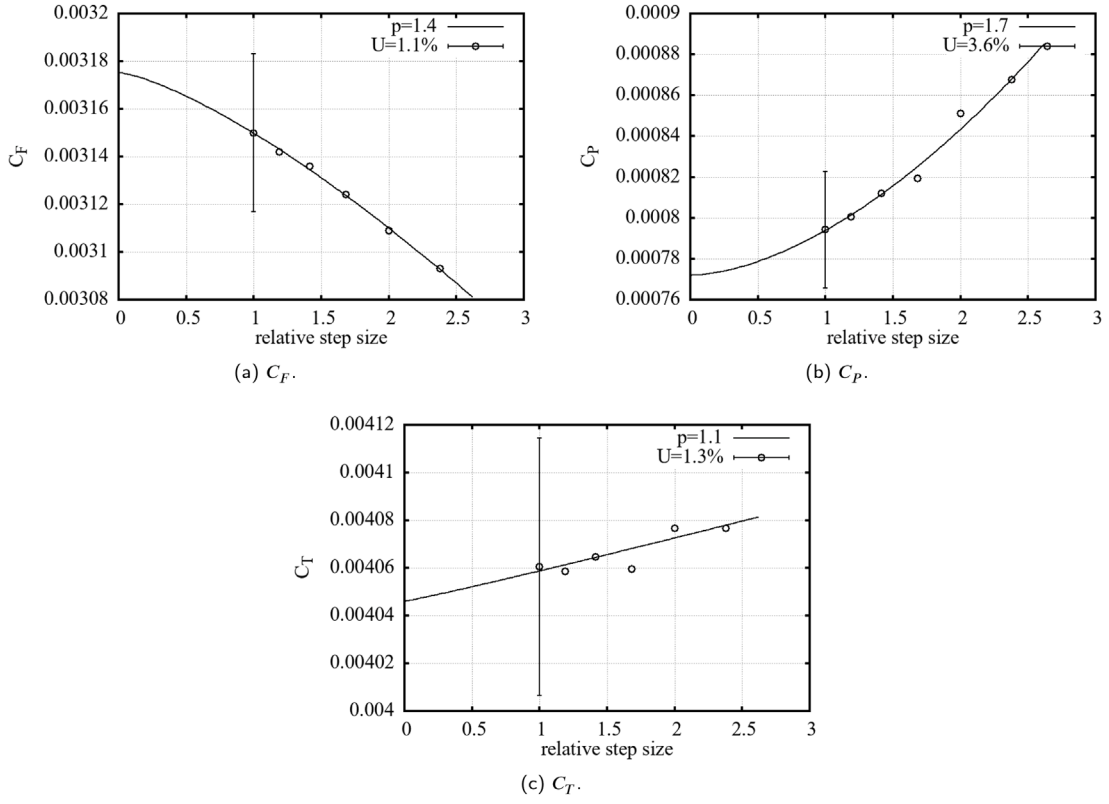

Fig. 2. Grid convergence of frictional, viscous pressure and total resistance coefficients, self-propelled case, model-scale.

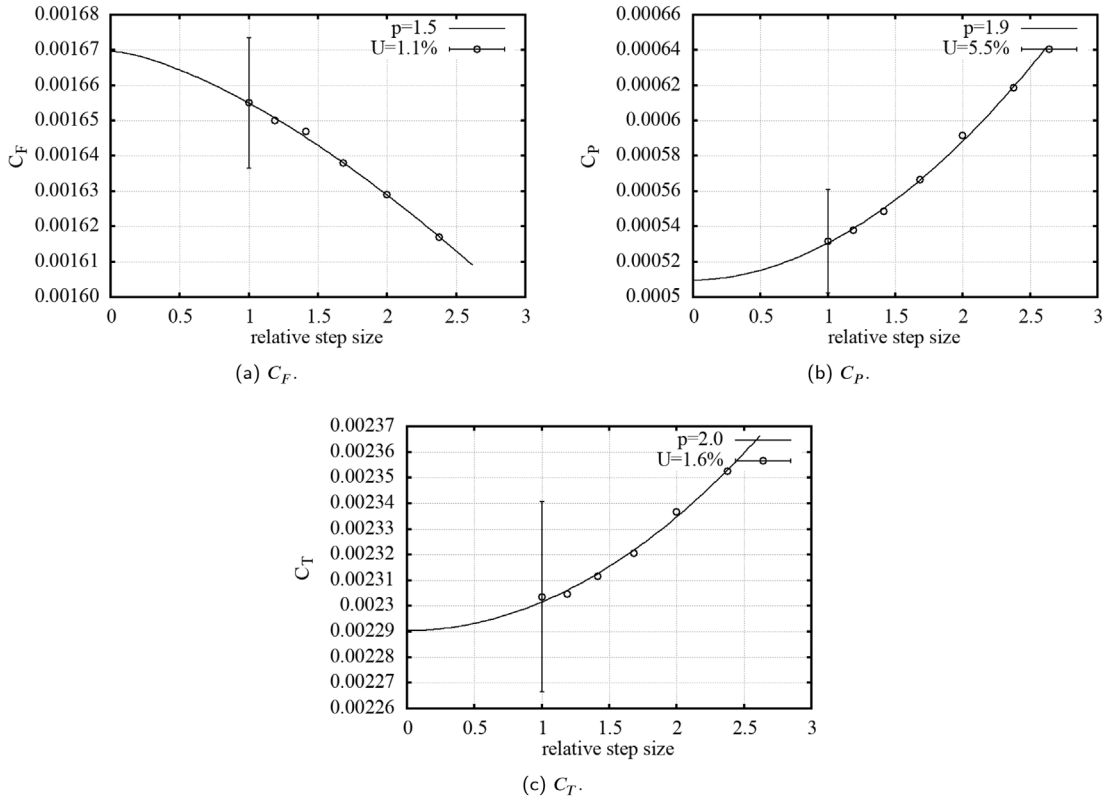

Fig. 3. Grid convergence of frictional, viscous pressure and total resistance coefficients, self-propelled case, full-scale.

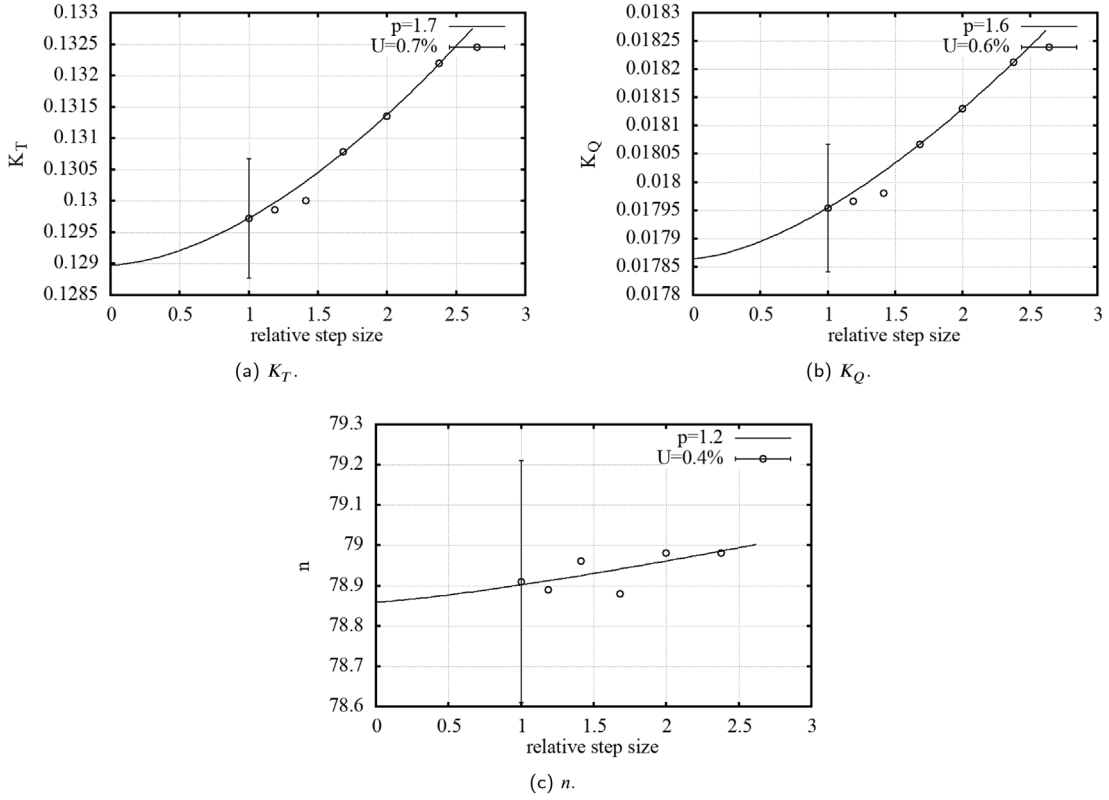

(a) K_T. (b) K_Q. (c) n.

Fig. 4. Grid convergence of propulsive factors, full scale.

Table 9
Propulsive factors, full scale.

Grid	K_T	$K_Q \times 10^{-1}$	n [rpm]	P_D [MW]
1	0.1297	0.1795	78.91	3.055
2	0.1299	0.1797	78.89	3.054
3	0.1300	0.1798	78.96	3.066
4	0.1308	0.1807	78.88	3.070
5	0.1313	0.1813	78.98	3.093
6	0.1322	0.1821	78.98	3.108
p	1.7	1.6	1.2	2.0
$U_G\%S_1$	0.7	0.6	0.4	1.4

Table 10
Uncertainty and deviations of delivered power, full scale.

Grid	$n_g \times 10^6$	P_D [MW]	$U_G\%S_i$	$\lvert P_{Di} - P_{D0}\rvert \% P_{D0}$
0	∞	3.040	–	–
1	44.14	3.055	1.40	0.49
2	26.61	3.054	1.92	0.45
3	16.26	3.066	2.56	0.85
4	9.97	3.070	3.65	0.98
5	6.02	3.093	5.03	1.74
6	3.77	3.108	6.90	2.23

6. Validation

The computations for the verification part are performed with some simplifications to isolate potential sources of scatter in the numerical solution. To validate the computed results with the measurements the ship geometry and conditions have to be represented as accurately as possible and the missing drag sources need to be recognized and included in the final results. The roughness effects on the hull and propeller at full scale are computed using the model implemented in the RANS code. The aerodynamic resistance is added using the ship frontal area and a coefficient provided by the model testing facility. There is also an addition of the bilge keel drag.

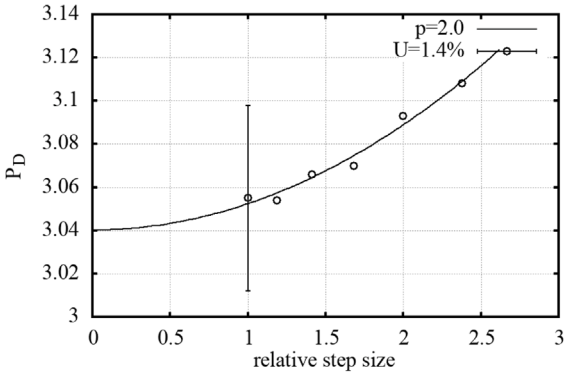

Fig. 5. Grid convergence of delivered power, full-scale.

Considering the computational effort the fourth finest grid is used in the validation. The delivered power difference between the finest setup with over 44 $\times$ 10^6 cells and the selected one with about 10 $\times$ 10^6 is less than 0.5%, Table 10.

6.1. Hull roughness

The added resistance due to the hull roughness can significantly increase the power demand. Even a newly painted surface may exhibit roughness large enough to raise the fuel consumption a few percent compared to a hydraulically smooth surface.

The topological properties of the rough surfaces are often described with only a single parameter. One example used in ship hydrodynamics is the average hull roughness, *AHR*, see Townsin et al. (1981). In many CFD methods, the roughness models also use a single number description in the form of an equivalent sand roughness, k_S. The numerical models are often tuned to represent certain measurements.

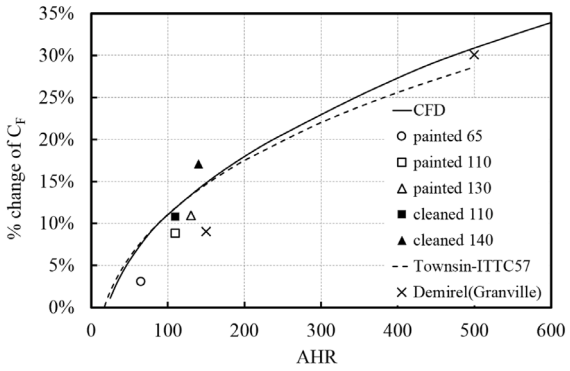

Fig. 6. Comparison of CFD simulations ($AHR/k_S = 5$) with Granville/Grigson extrapolated rough flat plates and Townsin estimated increase of C_F. KCS conditions, L = 230 m, $Rn = 2.89 \times 10^9$.

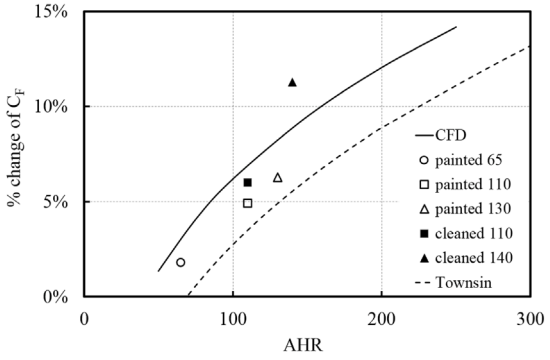

Fig. 7. Comparison of CFD simulations ($AHR/k_S = 5$) with Granville/Grigson extrapolated rough flat plates and Townsin estimated increase of C_F. Current hull conditions, L = 180 m, $Rn = 9.7 \times 10^8$.

Therefore, there is a large number of models available and more are being developed to suit specific surface types and conditions. Some of them were studied in Orych et al. (2021), where their different behaviours were presented. For the currently available models, the remaining challenge is the correlation between the two measures, namely AHR and k_S.

In the ITTC extrapolation method, Townsin's formula for added resistance due to roughness is used, ITTC (2017b). It is quite instinctive for a naval architect to cross-check the CFD results against this solution. Plotting the increase in frictional resistance as a function of average hull roughness, $\Delta C_F(AHR)$, based on Townsin's method together with computed increase as a function of equivalent sand roughness, $\Delta C_F(k_S)$, should help to find the relation between the AHR and k_S. As the first example, a flat plate with length and speed corresponding to the Kriso Container Ship (KCS), Hino et al. (2020), is considered. Using the AHR/k_S factor of 5 yields nearly perfect correlation between the Aupoix-Colebrook model, Aupoix (2014) and Townsin's method up to the suggested maximum of 230 μm for the latter one, see Fig. 6. However, repeating the exercise for the present ship, which is shorter and slower, the results are disappointing. Quite different curves are noticeable in Fig. 7. Decreasing length and speed further, shows that the roughness limit for a "hydraulically smooth surface" based on Townsin's formula is unreasonably high and may lead to underestimation of the resistance due to roughness in such applications.

The second approach to find the AHR/k_S correlation is based on experimental results for a flat plate. The measurements of several painted surfaces are extrapolated to full-scale length with Granville's method and to appropriate speed with Grigson's method with help of SSPA's Skin Friction Database tool, Leer-Andersen (2020). In this case, both newly painted plates and cleaned ones after deployment in the sea are used. The AHR for these samples is from 65 to 140 μm. For the same correlation factor that seemed to be suitable for Townsin's formula in case of the conditions similar to the KCS, the extrapolated measured values and CFD results show a good level of consistency for both ships, Figs. 6 and 7. Considering the fact that the experiments which constitute the basis of the roughness models implemented in the CFD code are based on different surface roughness types, the agreement is satisfactory and seems more reliable than Townsin's formula. For the KCS case, the results from other extrapolated measurements described by Demirel et al. (2017) are shown in Fig. 6.

It has to be highlighted that there is no universal AHR/k_S correlation factor, not only due to the numerical models but also since the rough surface topology cannot be adequately represented by a single number. A good example of that is the significant difference in C_F change between the newly painted, aged and subsequently cleaned surfaces with the same AHR, which can also be seen in the figures. The full-scale data considered in this work is based on delivered power measurements of ships during sea trials. The average hull roughness was reported but there is no detailed description of the surface texture. Therefore, the Aupoix-Colebrook roughness model with $AHR/k_S = 5$, which indicates conservative values of resistance increase is selected.

6.2. Full-scale measurements and post-processing

It is notoriously difficult to obtain sea trial data from a shipowner by a third party. Even more problematic is to get good quality materials with accurate measurements and proper records of the procedure. In this case, the authors are fortunate to gain access to a well-documented set of measurements for 12 sister ships.

The trials are performed according to the ITTC procedure, ITTC (2017c), also included in ISO 15016 standard. Three power settings are included and data acquired for power, speed, propeller rate of revolution, wind, waves, current and temperature, among others. Corrections are applied for wind, waves, current and temperature effects. In connection to the trial runs the Average Hull Roughness is measured.

Three sister vessels are selected based on the conditions during the measurements. These are tested at design draught in nearly perfect weather conditions, which minimize the measurement and correction errors. Therefore, the resulting measurement uncertainty is at a level allowing for proper validation of the CFD simulations.

6.3. Full-scale predictions

The most important part of this investigation is a full-scale self-propulsion simulation. It is performed at speeds of 12.5, 13.5 and 14.5 knots. This range includes the available sea trial runs for the selected cases. In the computations, the roughness effects are taken into account and the AHR is set to 100 μm, according to the average of the measured values. The windage is computed using the frontal ship area and a resistance coefficient suggested by the towing tank performing the model tests. To estimate the drag of the bilge keels, their wetted area and the frictional resistance coefficient for the bare hull are used. Both are added as an additional resistance during the self-propulsion simulation. To account for the propeller roughness a value of 30 μm, indicated by ITTC extrapolation method is used. The delivered power from the sea trials and SHIPFLOW simulations are presented in Fig. 8.

The curve fitting of the sea trial data is done according to the ITTC recommendations, ITTC (2017c). Thus, a curve representing the mean value of the two available towing tank predictions is shifted vertically such that the Root-Mean-Square (RMS) error of the data points is minimized. The Normalized RMS Error is 2.8%. Included in the plot are also the uncertainties estimated for the sea trials and the CFD results. A band of ±6.1% represents the experimental uncertainty, U_D, which can be expected from these sea trials. It is computed based on the sea trial uncertainties presented by Werner and Gustafsson (2020), where, for

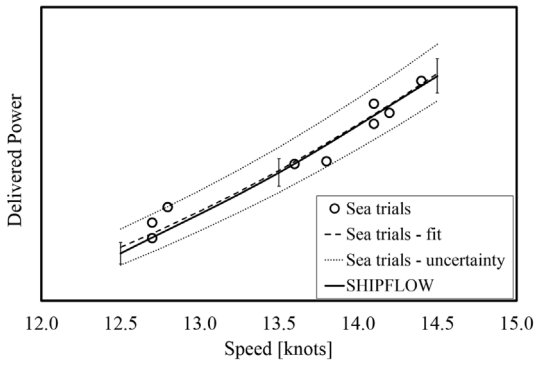

Fig. 8. Delivered power for sea trials and CFD simulations.

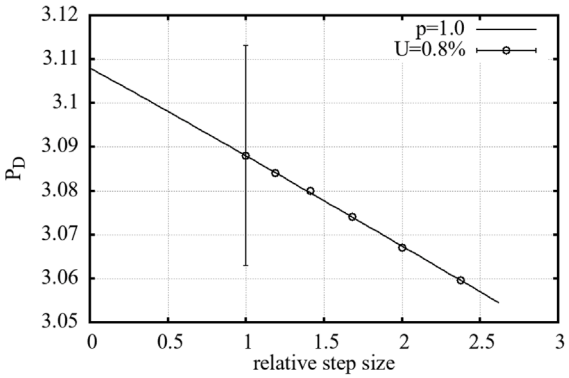

Fig. 9. Potential flow grid variation. Effect on delivered power.

Table 11
Measurement uncertainty and differences between CFD simulations and sea trial data fit for delivered power.

Speed	P_D	
[knots]	$\|E\|$%D	U_{Val}%D
12.5	1.9	7.1
13.5	0.6	–
14.5	0.5	–

good weather conditions during trials, the precision uncertainty is 8% for each individual point. The uncertainty of the mean value is obtained by dividing by the square root of the number of sister ships, Farrance and Frenkel (2012), resulting in a precision error, P, of 4.6% for this case. Furthermore, according to, Insel (2008) the expected bias error, B, for delivered power is at a level of 4%. P and B can be combined to obtain $U_D = \sqrt{P^2 + B^2}$. As it can be recalled from the verification part in this paper, the delivered power numerical uncertainty, U_{SN}, is 3.65% for the grid size used in the simulations. It is estimated at 12.5 knots of speed and is assumed to be similar at 13.5 and 14.5 knots.

According to the ITTC (2017d) a computation is considered validated at the U_{Val} level if the comparison error, $|E|$, is smaller than U_{Val}:

$$|E| < U_{Val} = \sqrt{{U_{SN}}^2 + {U_D}^2}$$

To assess the comparison error of the validation, E, the differences between computed results and the sea trial data fit are calculated and expressed in percent of the latter one, D, Table 11. The computed delivered power errors are much smaller than the validation uncertainty. Therefore, the simulations may be considered validated at the U_{Val} level (7.1%). It is worth noting that the numerical uncertainty is lower than, and entirely within, the experimental uncertainty.

No validation of the propeller rate of revolution is presented since there is not sufficient data to estimate the bias error and there is a strong impression that the propeller pitch was modified compared to the initial design to adjust the RPM to better match the engine characteristics.

7. Discussion

There are three types of errors in a computation, Coleman (2009): numerical errors, physical modelling errors and errors in input data. The numerical errors (including discretization scheme) are investigated through grid dependence studies. The physical errors stem from different sources: turbulence model, boundary conditions, propeller model, free surface approximation, roughness modelling and in the present case the modelling of bilge keels, and air resistance. The input data errors are related to the CAD description of the hull. All these errors but the turbulence model and the boundary conditions are discussed here.

The grid dependency study presented in Verification section is done only for the RANS part of the solution. The wave resistance is computed with a separate potential flow method. In the verification and the validation described earlier, it is computed with a mesh that is set up based on many validations carried out since the method was developed. To complete the study and quantify the uncertainties associated with the potential flow solution a series of six meshes is prepared ranging from 9409 to 53 908 panels. The upper limit of this range is set by the onset of wave breaking and therefore inevitable convergence issues. This series of potential flow meshes is combined with the RANS grid with 10×10^6 cells. The P_D uncertainty due to the potential flow mesh size is in this setup 0.81% for the finest mesh, see Fig. 9. For the validation part where the fourth finest RANS and potential flow solutions are used the total P_D uncertainty is 3.90%. It is evaluated using the root sum of the squares with contributions from the viscous part that is 3.65% and potential flow part, 1.38%. Therefore, the uncertainty increase of 0.25% associated with the potential flow part of the solution does not change the overall conclusions. This is also in part due to the small wave resistance contribution to the total resistance, approximately 5% at 12.5 knots speed.

The numerical uncertainty includes both grid and iterative uncertainties. However, the simulations are carried out with very strict convergence criteria until the iterative errors are insignificant. For the grid with 10×10^6 cells the standard deviations of the integrated values calculated for the last 10% of iterations are below 0.03% for C_P, 0.01% for C_T, 0.005% for C_F, K_T, K_Q, n and P_D. This indicates that the iterative uncertainty is very small, and it is not included in the analysis.

When it comes to the hull roughness, the uncertainties lay on both experimental and numerical sides. The measured Average Hull Roughness is a single number that describes the hull condition. It does not take into account the local surface geometry, which influences the efficiency of the roughness elements to create disturbance in the flow. As seen in Figs. 6 and 7, a surface with the same AHR can give noticeably different resistance depending on whether the hull was freshly painted or cleaned. Also, the paint type would affect the resistance. The current numerical methods usually use an equivalent sand roughness that is not universally translatable from AHR. For these reasons, it is important to check how large an effect the AHR and AHR/k_S correlation factor would have on the results. Here, the AHR is varied by ±25% which is a spread between sister ships observed in the measurements. If this variation is associated with the correlation factor it creates an envelope in the change of C_F that contains all of the markers in Figs. 6 and 7. The delivered power change due to this variation is ±1.5%.

A similar study is also applied to the propeller roughness. This is realized by modification of the blade frictional coefficient introduced to the lifting line. The nominal propeller roughness is varied by as much as ±20% corresponding to the blades C_F change of ±5%. This results in ±0.9% difference in delivered power.

The estimation of air resistance is approximate as there are no wind tunnel measurements available. However, the air resistance is just 2.5% of the total resistance and therefore the contribution to the total uncertainty is expected to be less than 0.25% assuming the range of possible air resistance coefficients. In the same way, the resistance from the bilge keels is only roughly estimated. They contribute to 0.7% of the total resistance and the uncertainty introduced by this coarse approximation is considered marginal.

At the simulation preparation stage, it became obvious that the hull geometry described in the CAD model is not smooth and requires small corrections. This is not uncommon, and the computed hull shape and the built ship differ slightly. Furthermore, there is a small change introduced at the stern to the otherwise similar sister ships after several completed builds. This means that two slightly different hulls are used in the selected sea trials. The differences between the original, smoothened and modified hull shapes are investigated with CFD and the delivered power discrepancy between them is about 1.3%.

The above complementary studies of sensitivity to several important simulation parameters substantiate the confidence in the validity of the achieved numerical predictions accuracy at full scale.

8. Conclusions

The main objective of this paper is to present a validation of CFD simulations of delivered power for a full-scale ship. In addition, a verification of the numerical method through systematic grid refinement studies is presented both for model-scale and full scale. Numerical uncertainties are determined for the total resistance and its components, the propulsive factors, and the delivered power. The numerical uncertainty of the delivered power at model scale is 2.3% and at full-scale 3.7% for a medium size grid with ten million cells. In the full-scale validation, special emphasis is placed on the effect of the surface roughness, both of the hull and the propeller. The validation is based on sea trial results, where the experimental uncertainty is estimated to 6%. Together with the numerical uncertainty this gives a validation uncertainty of 7%. For the speed range from 12.5 to 14.5 knots the average comparison error is 1%, i.e. considerably smaller than the validation uncertainty.

CRediT authorship contribution statement

Michal Orych: Conceptualization, Methodology, Software, Validation, Visualization, Writing – original draft. **Sofia Werner:** Data Curation, Writing - review & editing. **Lars Larsson:** Supervision, Writing – review & editing.

Declaration of competing interest

Michal Orych reports financial support was provided by Energimyndigheten (Swedish Energy Agency). Michal Orych reports a relationship with FLOWTECH International AB that includes: board membership and employment.

Acknowledgements

The authors would like to thank: Energimyndigheten (Swedish Energy Agency) for the financial support and SSPA for providing highly valuable input on full-scale measurements. The computations were enabled by resources provided by the Swedish National Infrastructure for Computing (SNIC) at C3SE, partially funded by the Swedish Research Council through grant agreement no. 2016-07213.

References

Aupoix, B., 2014. Wall roughness modelling with $k-\omega$ SST model. In: 10th International ERCOFTAC Symposium on Engineering Turbulence Modelling and Measurements, Marbella, Spain.

Broberg, L., Regnström, B., Östberg, M., 2007. XCHAP – Theoretical Manual. FLOWTECH International AB, Gothenburg, Sweden.

Chakravarthy, S., Osher, S., 1985. A new class of high accuracy TVD schemes for hyperbolic conservation laws. In: 23rd Aerospace Sciences Meeting, Reno, NV, U.S.A.. AIAA paper No 85–0363.

Coleman, H., 2009. ASME V&V 20-2009 Standard for Verification and Validation in Computational Fluid Dynamics and Heat Transfer. The American Society of Mechanical Engineers, New York.

Demirel, Y.K., Turan, O., Incecik, A., 2017. Predicting the effect of biofouling on ship resistance using CFD. Appl. Ocean Res. 62, 100–118.

Deng, G.B., Queutey, P., Visonneau, M., 2005. Three-dimensional flow computation with Reynolds stress and algebraic stress models. In: Procedings of the ERCOFTAC International Symposium on Engineering Turbulence Modelling and Measurements; ETMM6, Sardinia, Italy, 23–25 May, 2005. pp. 389–398.

Dick, E., Linden, J., 1992. A multigrid method for steady incompressible Navier-Stokes equations based on flux difference splitting. Internat. J. Numer. Methods Fluids 14, 1311–1323.

Eça, L., Hoekstra, M., 2014. A procedure for the estimation of the numerical uncertainty of CFD calculations based on grid refinement studies. J. Comput. Phys. 262, 104–130.

Eça, L., Hoekstra, M., Raven, H., 2010. Quantifying roughness effects by ship viscous flow calculations. In: 28th Symposium on Naval Hydrodynamics, Pasadena, California, September 16, 2010.

Farrance, I., Frenkel, R., 2012. Uncertainty of measurement: A review of the rules for calculating uncertainty components through functional relationships. Clin. Biochem. Rev. 33, 49–75.

Hino, T., Stern, F., Larsson, L., Visonneau, M., Hirata, N., Kim, J., 2020. Numerical Ship Hydrodynamics. An Assessment of the Tokyo 2015 Workshop. In: Lecture Notes in Applied and Computational Mechanics, vol. 94, Springer Nature, Switzerland, http://dx.doi.org/10.1007/978-3-030-47572-7.

Hochkirch, K., Mallol, B., 2013. On the importance of full-scale CFD simulations for ships. In: 12th Conf. Computer and IT Applications in the Maritime Industries (COMPIT), Cortona, Italy. pp. 85–95.

Insel, M., 2008. Uncertainty in the analysis of speed and powering trials. Ocean Eng. 35, 1183–1193.

ITTC, 2017a. 1978 ITTC Performance Prediction Method, ITTC Quality System Manual, Recommended Procedures and Guidelines. Propulsion Committee of the 28th ITTC.

ITTC, 2017b. Proceedings of 25th ITTC – Volume II, Final Report and Recommendations to the 25th ITTC. The Specialist Committee on Powering Performance Prediction, Fukuoka, Japan.

ITTC, 2017c. Preparation, Conduct and Analysis of Speed/Power Trials, ITTC Quality System Manual, Recommended Procedures and Guidelines. Specialist Committee on Ships in Operation at Sea of the 29th ITTC.

ITTC, 2017d. Uncertainty Analysis in CFD Verification and Validation Methodology and Procedures, ITTC Quality System Manual, Recommended Procedures and Guidelines. Resistance Committee of the 28th ITTC.

Janson, C.-E., 1997. Potential Flow Panel Methods for the Calculation of Free-Surface Flows with Lift (Ph.D. thesis). Chalmers University of Technology, Gothenburg, Sweden.

Kim, K., Leer-Andersen, M., Orych, M., 2014. Hydrodynamic optimization of energy saving devices in full scale. In: Proceedings, 30th Symposium on Naval Hydrodynamics, Hobart, Tasmania, Australia.

Korkmaz, K.B., 2015. CFD Predictions of Resistance and Propulsion for the JAPAN Bulk Carrier (JBC) with and Without an Energy Saving Device (MSc Thesis). Chalmers University of Technology, Gothenburg, Sweden.

Leer-Andersen, M., 2020. Skin friction database. https://www.sspa.se/tools-and-methods/skin-friction-database/extrapolation-full-scale.

MARIN, 2018. Numerical Uncertainty Analysis – User Manual. MARIN, The Netherlands.

Orych, M., Werner, S., Larsson, L., 2021. Roughness effect modelling for wall resolved RANS – comparison of methods. in preparation.

Pereira, F., Vaz, G., Eça, L., 2017. Verification and validation exercises for the flow around the KVLCC2 tanker at model and full-scale Reynolds numbers. Ocean Eng. 129, 133–148.

PETSc, 2020a. PETSc web page. https://www.mcs.anl.gov/petsc/index.html.

PETSc, 2020b. PETSc documentation, solvers. https://www.mcs.anl.gov/petsc/petsc-current/docs/manualpages/KSP/KSPGMRES.html.

PETSc, 2020c. PETSc documentation, preconditioners. https://www.mcs.anl.gov/petsc/petsc-current/docs/manualpages/PC/PCBJACOBI.html.

Ponkratov, D., 2017. 2016 workshop on ship scale hydrodynamic computer simulations. In: Proceedings: Lloyd's Register's Full-Scale Numerical Modelling Workshop.

Raven, H.C., van der Ploeg, A., Starke, A., Eça, L., 2008. Towards a CFD-based prediction of ship performance —progress in predicting full-scale resistance and scale effects. Trans. RINA A 150, 31–42.

Roe, P.L., 1981. Approximate Riemann solvers, parameter vectors, and difference schemes. J. Comput. Phys. 43, 357.

Townsin, R., Byrne, D., Svensen, T., Milne, A., 1981. Estimating the technical and economic penalties of hull and propeller roughness. Trans. Soc. Nav. Archit. Mar. Eng. 89, 295–318.

Werner, S., Gustafsson, L., 2020. Uncertainty of speed trials. In: Proceedings of the HullPIC 2020, Hamburg, Germany. pp. 26–28.

Zhang, D.H., 1990. Numerical Computation of Ship Stern/Propeller Flow (Ph.D. thesis). Chalmers University of Technology, Gothenburg, Sweden.